# CHAPTER 6

# MORPHOLOGIES OF POLY(ε-CAPROLACTONE) DENDRITES: EFFECTS OF MULTIPLE HYSTERESIS CYCLES, COMPRESSION RATE AND "DEGREE OF UNDERCOOLING"

## 6.1. Abstract

In Chapter 5, the morphological details of structures formed in blends of poly(ε-caprolactone) (PCL) and poly(t-butyl acrylate) (PtBA) Langmuir films at the air/water (A/W) interface during dynamic compression experiments were discussed. Nonequilibrium growth of PCL compositional dendrites were observed during dynamic compression experiments. In this chapter, the morphological evolution of PCL dendrites for multiple hysteresis loops, different compression rates, and isobaric (constant surface pressure, Π) experiments for a representative PCL/PtBA blend with a PtBA mole fraction of $X_{PtBA} \sim 0.14$ will be explored. The results obtained from Brewster angle microscopy (BAM) and surface pressure-average area per monomer (Π-<A>) isotherm studies indicate that the compositional dendrites of PCL were not formed during second compression cycles in multiple hysteresis loop experiments. Dynamic compression experiments performed at various compression rates demonstrate that increasing compression rate suppresses PCL crystallization and leads to smaller dendritic crystals at similar <A>. This observation is consistent with the compression rate dependent studies performed for single-component PCL Langmuir films in Chapter 4. On the other hand, the morphologies of compositional PCL dendrites observed during isobaric area relaxation experiments at different Π values demonstrate a transition from highly

branched symmetric dendrites, to six-arm dendrites, four-arm dendrites, seaweedlike crystals and distorted rectangular crystals. In this study, Π in isobaric experiments, analogous to temperature in bulk isothermal crystallization studies, has a profound impact on morphology because of the interplay between diffusion, interfacial energy, and the anisotropy of interfacial energy. Extensive morphological studies of PCL dendritic crystals grown in PCL/PtBA blends as Langmuir films provide a model system to further investigate pattern formation of polymer crystals grown in diffusion-limited regimes.

## 6.2. Introduction

Dendritic growth of condensed phases is a nonequilibrium solidification process and strongly depends on the growth conditions. Over the past several decades, dendritic growth for small molecules has been widely studied and several models have been developed to understand growth mechanisms;[126-128] however, relatively little was known about dendritic growth in polymeric systems until recently.[9, 11-19, 118]

Several studies were carried out to examine the crystallization of semicrystalline poly(ethylene oxide) (PEO) in thin film geometries. Dendritic growth of PEO crystals was observed as PEO film thickness approaches ~ 10 nm in contrast to single crystal and spherulitic crystal morphologies observed in thicker films.[11-16] Furthermore, adding amorphous poly(methylmethacrylate) (PMMA) into PEO has been used to "tune" the crystal morphology of PEO in mixed thin films.[19, 118] Dendritic growth of polymer crystals in thin film geometries is not limited to studies of PEO. Taguchi *et al.* extensively investigated the crystal growth of isotactic polystyrene (it-PS) in ~ 11 nm thick films.[122] Dendritic crystals with sixfold symmetry and compact seaweed morphologies were observed with decreasing crystallization temperature. Another frequently used model polymeric system for crystallization studies is poly(ε-

caprolactone) (PCL). Crystallization of PCL and PCL-based polymer blends in spincoated thin film geometries have been studied.[8-10] The growth rate of PCL crystals was found to be roughly one-half the bulk growth rate at crystallization temperatures of 50 °C and 54 °C for 15 nm thick films.[9] In contrast, 6 nm thick films exhibit drastically slower growth rates which are comparable at both temperatures. However, as film thickness increases, bulk crystallization rates are recovered. For example, the growth rates observed for PCL films with thicknesses in the range of 30-200 nm at both 50 °C and 54 °C are consistent with measurements for thicker films up to 2000 nm and bulk crystallization.[9] Like the PEO case discussed above, dendritic morphologies are also observed in 9 nm or thinner PCL spincoated films on silicon substrates.[9]

Generally speaking, dendritic growth is driven by the Mullins-Sekerka instability.[126] This type of interfacial instability causes small protrusions to form at the interface between growing crystals and the surrounding liquid phase. The advancing growth front of a protrusion disturbs the nearby diffusion field in the supersaturated or supercooled liquid phase and leads to a locally higher growth rate of the apex in the protrusion. Meanwhile, growth in the interfacial region near the protrusion is hindered because heat or solvent molecules tend to accumulate in this region. Therefore, the small protrusion grows faster and eventually gives rise to a dendritic finger. This type of interfacial instability is most commonly observed in a diffusion fields caused by either thermal or concentration gradients around the growth fronts of the solid phase.[126, 127]

While the Mullins-Sekerka instability favors dendritic structures, surface tension acts to stabilize the interface. As a result, anisotropy of the surface tension can influence the growth direction and morphologies of crystals in thin film systems. Diffusive properties of molecules together with the effects of the anisotropy of the surface energy ultimately

determine the growth rate and morphologies of crystals. Although the anisotropy of surface energy is an important factor to determine the gross morphology, it cannot be directly measured by experiments. However, the anisotropy of the surface energy is an important adjustable parameter in theoretical studies. As an example, Kyu and coworkers used the surface energy anisotropy to simulate morphological transitions in it-PS thin films at various degrees of undercooling.[130] Both the experimental observations and simulation results demonstrate similar morphological transitions from hexagonal single crystals to dendritic crystals and finally nonfaceted branched morphologies for increasing degrees of undercooling and decreasing anisotropy of the surface energy.[122, 130]

Other parameters such as molar mass, composition, undercooling, etc. also affect the dendritic growth of polymer crystals through their influence on the characteristic diffusion length. The characteristic diffusion length is given by $l = 2D/\nu$, where D represents self-diffusion coefficient of polymer chains and ν is growth rate. The diffusion coefficient usually decreases with decreasing temperature as reviewed in Chapter 2, while growth rate increases with decreasing crystallization temperature. For example, in it-PS thin film systems, the diffusion length decreases dramatically with decreasing crystallization temperature, leading to a decrease in the width of sidebranches at higher degrees of undercooling.[122]

All of the parameters discussed above exert their influences on dendritic growth in a diffusion field near the interface between a liquid and a growing crystal. The diffusion field is commonly generated by either thermal or concentration gradients. However, as pointed out by Taguchi *et al.*, the thermal diffusion may not give rise to interfacial instabilities in polymeric systems because the growth rate is usually too slow to compete

with the thermal diffusion length.[122] As a result, the effect of thermal diffusion can be ignored. Meanwhile, for dendritic crystallization of single-component melts in thin films, simple concentration gradients can be ruled out. Taguchi and coworkers indicated that the diffusion field is generated by the gradient of melt thickness from the edge of the growing crystals to the surrounding polymer melts, which destabilizes the interface and leads to the formation of dendritic branches. However, thickness gradients of polymer melts can be converted to the surface concentration of polymer chains. Thus, this type of diffusion field can still be correlated to the concentration gradient and analyzed accordingly. Nevertheless, a full understanding of the dendritic growth for polymeric systems down to molecular level is still incomplete, though numerous studies have focused on this issue.[9, 11-19, 118]

For the aforementioned studies on dendritic growth of polymer crystals in thin film geometries, the polymer films are usually prepared on solid substrates by spincoating. On solid substrates, the cooperative motion of polymer chains directly affects chain folding and consequently the crystallization rate and morphology.[145] Furthermore, surface defects on solid substrates can affect the nucleation and growth mechanism for crystal growth. However, at the air/water (A/W) interface, ultrapure water minimizes surface defects, providing a model surface for probing crystallization in thin films.[24, 26] Even though the nonequilibrium growth of dendritic patterns in supersaturated Langmuir monolayers have been evaluated for small amphiphilic molecules N-dodecylgluconamide,[53] dioctadecylamine (DODA),[131] ethyl palmitate (EP),[131] ethyl stearate (ES),[131] diacetylene 10, 12-tricosadiynoic acid,[132] and D-myristol alanine.[133, 134] To the best of our knowledge, diffusion-limited growth of polymer crystals in Langmuir monolayers has only been observed for PCL-based systems.[24, 26]

Previous studies have shown that the nucleation and growth of PCL crystals in single component Langmuir films occurs in the meta-stable (supersaturated) monolayer regime at room temperature (T = 22.5 °C) just below PCL's dynamic collapse pressure of $\Pi_{C,PCL}$ ~ 11 mN·m$^{-1}$.[24, 26] In Chapter 5, we reported that PCL and poly(t-butyl acrylate) (PtBA) form compatible blends as Langmuir monolayers at $\Pi$ < ~ 10 mN·m$^{-1}$. For PCL-rich blends, *in situ* Brewster angle microscopy (BAM) studies reveal nonequilibrium growth of PCL crystals for compression past the PCL collapse transition. In the subsequent plateau regime PtBA is excluded from growing PCL crystals, presumably hindering PCL diffusion from the surrounding monolayer to the crystal growth fronts. As a result, PCL crystals exhibit dendritic morphologies. In contrast, PtBA-rich blend films suppress PCL crystallization. The compositional PCL dendrites can be transferred onto silicon substrates coated with spincoated polystyrene using the Langmuir-Schaefer (LS) method. Atomic force microscopy (AFM) cross-sectional analysis performed on the LS films shows crystal thicknesses for the PCL dendrites are ~ 7-8 nm, which is comparable to PCL crystals grown from single-component PCL monolayers.

In this chapter, a representative PCL (weight average molar mass, $M_w$ = 10 kg·mol$^{-1}$, polydispersity index, PDI = 1.25)/PtBA ($M_w$ = 25.7 kg·mol$^{-1}$, PDI = 1.08) blend with PtBA mole fraction of $X_{PtBA}$ ~ 0.14 is used to study the morphologies of PCL crystals grown at various experimental conditions. BAM is simultaneously performed during multiple hysteresis loop experiments to examine the effects of previous compression-expansion history on the re-crystallization of the PCL component during the second hysteresis loop. The hysteresis experiments were also carried out at various compression-expansion rates of 8, 16, 30, 130, and 200 cm$^2$·min$^{-1}$ to explore the compression rate dependence of PCL crystallization in Langmuir monolayers during

dynamic compression experiments. The morphologies of PCL dendrites were also captured by BAM during isobaric area relaxation experiments performed at target pressures of 11, 10.5, 10.3, 10, 9.5, and 8.5 $mN \cdot m^{-1}$. PCL crystals grown during isobaric area relaxation experiments were further transferred onto silicon substrates covered with spincoated polystyrene layer using the LS-method to obtain higher resolution morphological information relative to BAM from optical microscopy studies.

## 6.3. Results and Discussion

### 6.3.1. Effects of Previous Compression History (Re-crystallization) During Second Hysteresis Cycles

In Chapter 5, the dendritic growth of PCL crystals in PCL/PtBA blends during dynamic compression experiments has been examined in terms of blend composition. In order to gain further insight into the dendritic growth of PCL crystals in Langmuir films at different experimental conditions, two hysteresis loops were performed for a representative PCL/PtBA blend of $X_{PtBA} \sim 0.14$ to determine if the first hysteresis loop influences the crystal morphologies observed during a second compression step. During hysteresis experiments, the monolayer of PCL/PtBA blends was compressed to an average area per monomer of $\langle A \rangle \sim 10$ $Å^2 \cdot monomer^{-1}$ at a compression rate of 8 $cm^2 \cdot min^{-1}$, instead of compressing to the minimum trough area, to avoid damaging crystals by forced impingement during compression. The compressed blend films were then expanded to a maximum trough area of 700 $cm^2$ at the same expansion rate of 8 $cm^2 \cdot min^{-1}$. The monolayer was compressed again to $\langle A \rangle$ at $\sim 10$ $Å^2 \cdot monomer^{-1}$ and re-expanded to the trough area of 700 $cm^2$ at the same expansion rate of 8 $cm^2 \cdot min^{-1}$. The second compression experiment performed after the first hysteresis loop is analogous to a

"re-crystallization" process. BAM was simultaneously carried out to monitor the *in situ* morphologies of PCL crystals during hysteresis experiments.

Figure 6.1 clearly indicates that the second hysteresis loop (dotted line) does not retrace the first compression-expansion isotherm (solid line). Two distinct differences between the first and second hysteresis cycles are noted here: 1) the monolayer collapses at a lower Π value during the second compression step; and 2) the plateau Π value observed in the second expansion isotherm is slightly lower than that observed in the first expansion isotherm.

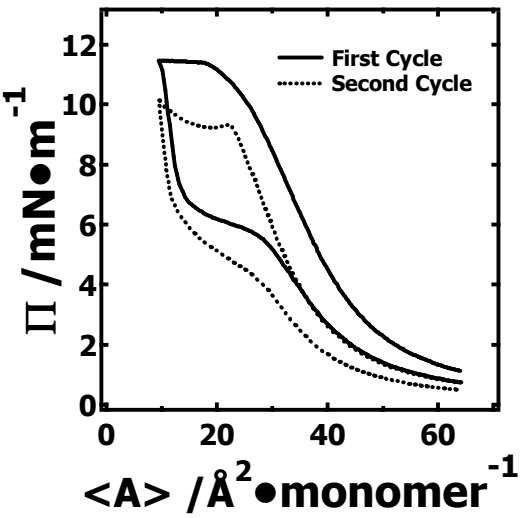


**Figure 6.1.** Two hysteresis loops for a PCL/PtBA blend of $X_{PtBA} \sim 0.14$. The isotherms were obtained at T = 22.5 $^{o}$C and a constant compression and expansion rate of 8 $cm^2 \cdot min^{-1}$. The solid line represents the first compression and expansion cycle. After the first hysteresis loop, the monolayer was immediately recompressed and expanded (dotted line). The second hysteresis loop was also carried out at a constant compression and expansion rate of 8 $cm^2 \cdot min^{-1}$.

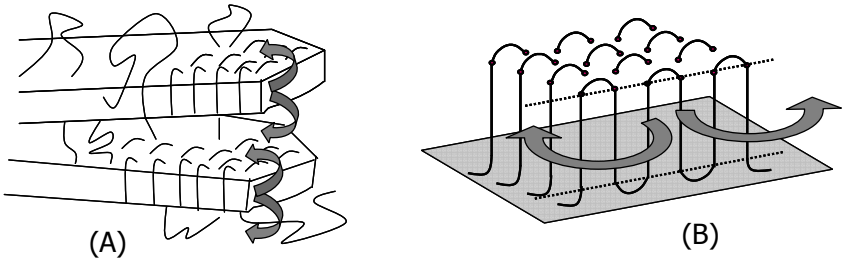


**Figure 6.2.** Rejection of amorphous components from crystallites indicated by dark arrows: (A) Edge-on lamellae with rejection occurring at the intralamellar region. (B) Flat-on lamellae with rejection occurring in the plane of crystal growth.

To fully understand the differences observed for the isotherms, crystallization and melting processes of PCL dendrites in PCL/PtBA blend Langmuir films during the first hysteresis cycle are briefly reviewed. The growth of PCL crystals starts once stable nuclei form as the blend films are compressed into the supersaturated monolayer region. Meanwhile, amorphous PtBA components are rejected from PCL crystallites. For polymer crystallization in semicrystalline-amorphous bulk blends, rejection of the amorphous components most commonly occurs at intralamellar regions as schematically depicted in Figure 6.2A. In contrast, in thin film geometries, the amorphous components have to be ejected in the plane of flat-on lamellar growth as indicated in Figure 6.2B.[118] Rejected amorphous components accumulate near crystal growth fronts instead of the intralamellar region. As a result, "phase separation" is triggered by further growth of semicrystalline components upon dynamic compression. This rejection process constrained in two dimensional (2D) geometries introduces interfacial instabilities associated with complicated mass diffusion fields near the crystal growth fronts, leading to various nonequilibrium growth morphologies.

Previous studies have already shown that the plateau region present in expansion isotherms corresponds to the melting of PCL crystals formed during compression.[24] An interpretation at the molecular level for this short plateau is that PCL chains start to detach from the crystals and diffuse back to the A/W interface as monolayers, allowing Π to remain relatively constant with increasing trough area while the crystals melt.[24, 26] However, after the first expansion (melting) step, chain conformations and mass distribution within the PCL/PtBA blends are not fully recovered. Therefore, many locally PCL-rich liquidlike domains and possibly even some solidlike nuclei may remain after the first hysteresis loop. If small 3D aggregates (locally well-ordered structure) remain at the end of the first hysteresis cycle, they can serve as nuclei for crystal growth upon the second compression step. Even though these small crystallites are too small to be observed by BAM with a linear resolution of 20 μm, it may be possible to infer their existence from morphological changes to crystals grown in the second compression step. Assuming preformed nuclei exist, PCL nucleation would be able to occur at smaller degrees of undercooling, corresponding to smaller Π values. Meanwhile, the second compression isotherm should shift to smaller <A> values because some of the PCL and possibly PtBA would already exist as multilayers during the second compression step.

As seen in Figure 6.1, both the dynamic collapse pressure, $\Pi_C$, and the <A> value where the collapse occurs shift to smaller values during the second compression step as expected for residual 3D structures at the end of the first hysteresis cycle. Furthermore, the lower plateau Π value observed in the second expansion isotherm indicates a slightly higher melting temperature and one could speculate that better chain organization exists in the crystals grown at a slightly lower degree of undercooling during the second

compression step. At this stage, it is useful to test the conclusions and explanation for the isotherms in Figure 6.1 with BAM studies.

Morphological studies for PCL dendrites grown during the first compression step for PCL/PtBA blend films like those shown in Figure 6.3 have been discussed in Chapter 5. That discussion will not be repeated here. Rather, Figure 6.3 is provided to highlight the differences seen in the second compression step (Figure 6.4). Figure 6.4A through 6.4C shows BAM images captured during the second compression step. It is clear that bright crystalline domains are present in these BAM images; however, these PCL crystals lack the multi-faceted features of crystals grown during the first compression step (Figure 6.3A through 6.3D) at similar surface concentrations. Meanwhile, the number of crystals formed during the second compression step is much greater than the first compression step. This observation is consistent with the hypothesis that many small well-ordered 3D domains remain at the end of the first hysteresis cycle and serve as nuclei for crystal growth during the second compression step. The absence of dendritic features for PCL crystals grown during the second compression step is possibly the result of two factors: 1) The size of crystals grown during the second compression step is too small to develop sidebranches; and 2) The crystallization of PCL during the second compression step essentially occurs in many small PCL-rich domains, which are locally separated by a PtBA-rich phase. The surface morphology of the PCL/PtBA blend films during the second hysteresis cycle is very similar to the behavior observed for single-component PCL Langmuir films discussed in Chapter 4.

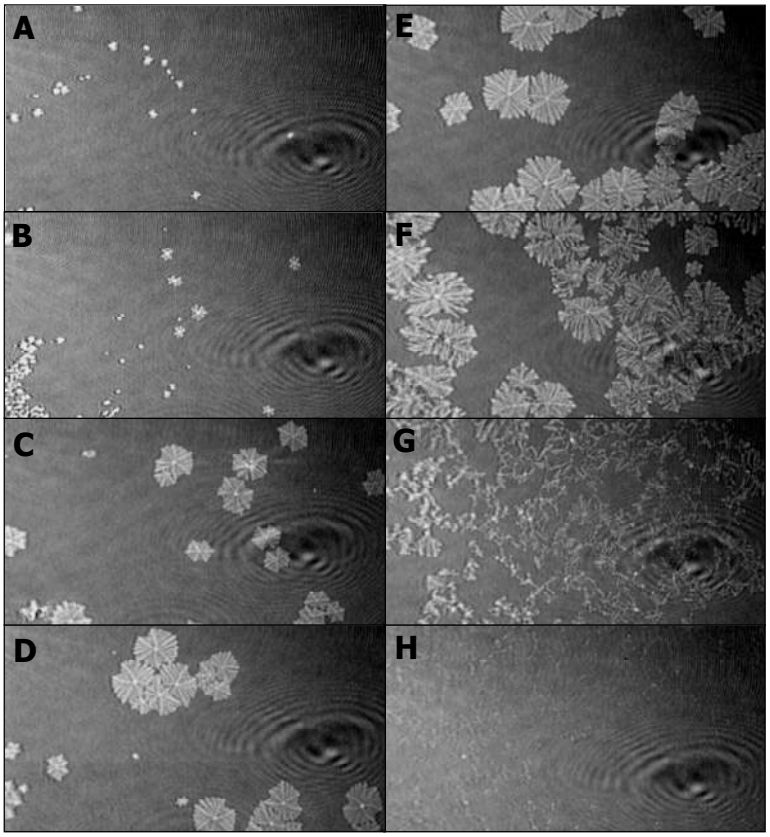


**Figure 6.3.** BAM images for a PCL/PtBA blend film of $X_{PtBA} \sim 0.14$ obtained at 22.5 $^{o}$C during the first hysteresis cycle. BAM images were taken during the first hysteresis experiments and correspond to (<A> /Å$^{2}$·monomer$^{-1}$) for compression: A (17.8), B (16.5), C (11.2), and D (10.1); and expansion: E (10.8), F (13.6), G (16), and H (22.7). Solid-like domains appear bright in all of the 4.8 × 2.6 mm$^{2}$ BAM images.

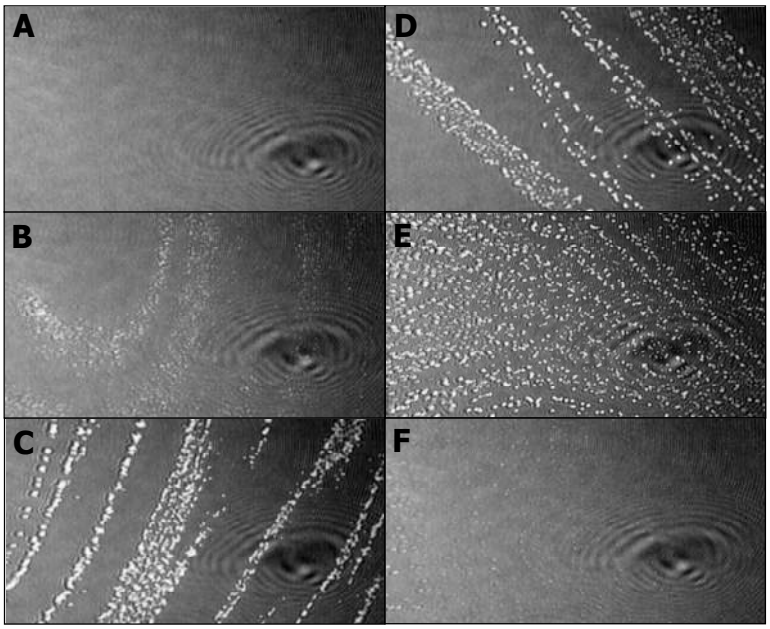


**Figure 6.4.** BAM images for a PCL/PtBA blend film of $X_{PtBA} \sim 0.14$ obtained at 22.5 $^{o}$C during the second hysteresis cycle. BAM images were taken during the second hysteresis experiments and correspond to (<A> /Å$^{2}$·monomer$^{-1}$) for compression: A (24.5), B (16.4), and C (11.8); and expansion: D (13.1), E (15.2), and F (24.5). Solid-like domains appear bright in all of the 4.8 × 2.6 mm$^{2}$ BAM images.

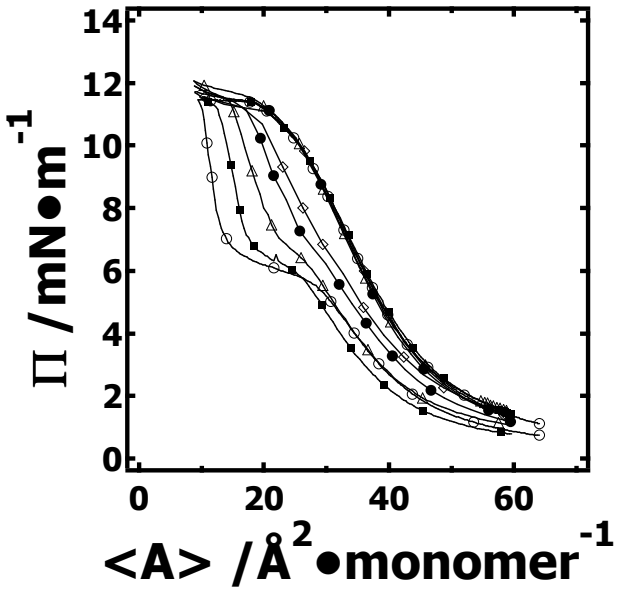


**Figure 6.5.** Π-<A> hysteresis loops for $X_{PtBA}$ ~ 0.14 PCL/PtBA blends obtained at T = 22.5°C for different compression rates: 8 (○), 16 (■), 30 (Δ), 130 (●), and 200 (◊) $cm^2 \cdot min^{-1}$.

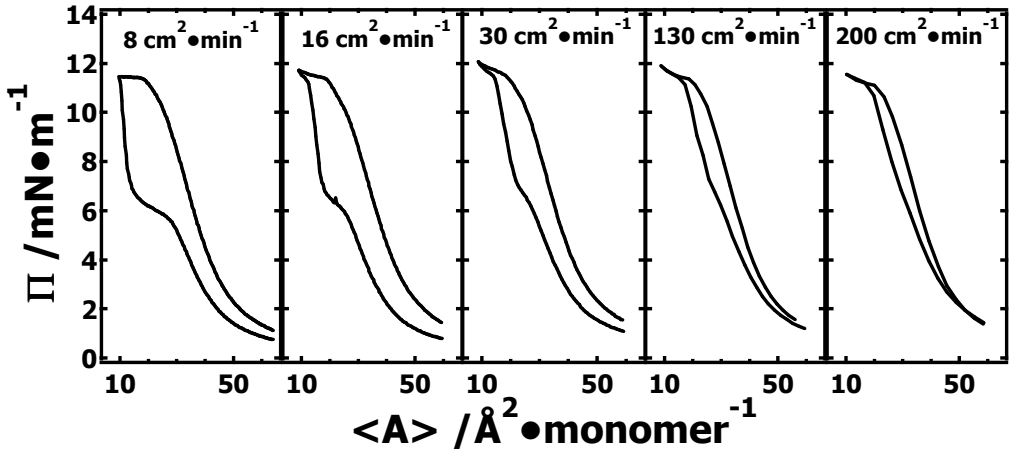


**Figure 6.6.** Π-<A> hysteresis loops for $X_{PtBA}$ ~ 0.14 PCL/PtBA blends obtained at T = 22.5°C for different compression rates: 8, 16, 30, 130, and 200 $cm^2 \cdot min^{-1}$.

### 6.3.2. Compression Rate (Quenching Rate) Dependence

It is known that the nucleation and growth of polymer crystals in bulk melts are affected by the quenching rate. Rapid quenching rates lead to smaller crystallites with poorer organized chain folded structures (lower degree of crystallinity) than those grown during slow cooling. A slower quenching rate assists the development of well-organized crystallites, which are thicker and melt at higher melting temperatures. At the A/W interface, the free energy barrier for nucleation and growth of stable nuclei is overcome by increasing surface pressure at a constant temperature during dynamic compression in the supersaturated monolayer region. Thus, compression rate, a surface analog to the quenching rate, should also affect the nucleation and growth of PCL crystals in Langmuir monolayers. Increasing the compression rate corresponds to increasing the quenching rate and should hamper the structural relaxation of polymer chains.

Figures 6.5 and 6.6 show Π-<A> hysteresis loops for $X_{PtBA}$ ~ 0.14 PCL/PtBA blends obtained at T = 22.5 °C for different compression and expansion rates. It is clear that no obvious difference was observed in the compression isotherms in the monolayer regime, although small differences exist in the vicinity of $\Pi_{C, PCL}$. However, a detailed discussion of this observation is not warranted as the differences are close to the measurements error (0.2 $mN \cdot m^{-1}$). In contrast to the compression step, substantial changes in the expansion isotherms with respect to compression rate are observed. First, the plateau Π value observed in the expansion isotherm increases with increasing compression rate from 8 to 30 $cm^2 \cdot min^{-1}$. For compression rates that are greater than 30 $cm^2 \cdot min^{-1}$, no distinct plateau region was observed. This observation could indicate that PCL crystallization is suppressed at high compression rates because the PCL chains lack sufficient time to order and form stable nuclei and/or crystallites. Such an interpretation is comparable to the

explanation of how a rapid cooling rate affects bulk crystallization. Previous studies have demonstrated that the plateau region in expansion isotherms is correlated to the melting process of crystals grown upon compression.[24, 26] A slightly elevated melting surface pressure, corresponding to a lower melting temperature, suggests poorer chain organization in PCL dendrites grown at higher compression rates (fast-quenching). Furthermore, the area inside hysteresis loop is qualitatively proportional to the heat released during crystallization and completely absorbed by water subphase. The more crystals that form and the better they are organized during compression, the greater the amount of heat that is released, leading to a larger hysteresis loop for same amount of PCL/PtBA blend. The area inside the hysteresis loop becomes smaller with increasing compression rate as seen in Figures 6.5 and 6.6, suggesting that PCL crystallization is suppressed by increasing compression rate. This observation is further confirmed by *in situ* BAM studies as shown in Figure 6.7.

In Figure 6.7, BAM images were captured at similar surface areas of <A> ~ 9-10 $Å^2 \cdot monomer^{-1}$ during compression experiments performed at different compression rates. The average size of PCL dendrites becomes smaller with increasing compression rate. At compression rates greater than 30 $cm^2 \cdot min^{-1}$, it is very hard to detect any dendritic branches because of the small crystal sizes and the limitation of BAM resolution. For PCL crystals grown during compression at 8, 16, and 30 $cm^2 \cdot min^{-1}$, it is desirable to estimate the overall growth rates from the BAM images. Unfortunately, this is not trivial and several approximations need to be made. Unlike measurements of growth rates from spherulites in bulk, where the radius of a single spherulite can be measured by optical or atomic force microscopy until it impinges upon its neighbors, crystals at the A/W interface are subject to flow. This complication means that it is impossible to keep a

crystal in the BAM's field of view over the crystal's entire lifetime. A second complication is that nucleation does not start at the same time for all crystals leading to a broad size distribution in any given BAM image. This complication is avoided in bulk measurements through the study of the same spherulite over its lifetime. Finally, there is also a large variation of growth rate from branch to branch even in one dendritic crystal. To overcome these problems, the following procedure is used to estimate the average growth rates: (1) The tip to tip diagonal distance (See Figure 6.8A) between two main dendritic trunks grown on the sector boundary lines for a given crystals serve as the linear dimension, L. However, an extra uncertainty must be considered due to the bending of the four main dendritic trunks during the compression process as seen in Figure 6.3 and Figure 6.7; (2) Typically, more than five crystals with representative sizes in a given image are measured. The exception to this is for BAM images possessing fewer than five crystals where all crystals are used. Crystals that were obviously much smaller or larger than average were not included. This cut-off is somewhat arbitrary, however, it is required so that measured crystals represent crystals that underwent nucleation at a similar time in each BAM image; and (3) The linear dimensions were then averaged and are plotted in Figure 6.8 as a function of the crystallization time with one standard deviation error bars. The time at which the measurable crystals first appear in the BAM field of view was considered to be the initial time, $t_0$. The time for each BAM image captured during the plateau region is considered as t. The crystallization time, $t_x$, for the crystals measured in these BAM images was computed as $t_x = t - t_0$. While the growth rates obtained from this procedure may not be ideal, it is the best that can be done at this time to estimate the average growth rate of PCL dendrites. The slopes from the empirical linear fits of L vs. $t_x$ in Figure 6.8B, $G = dL/dt_x$, yield the average crystal growth rates in

Table 6.1. While it is hard to make quantitative comparisons for these growth rates because of the measurement uncertainty, these values are much faster than dendritic growth of PCL crystals in spincoated films on silicon substrates.[9] Moreover, the growth rates are comparable for the three slowest compression rates. This observation indicates that the size differences observed in Figure 6.7 represent different $t_x$ rather than fundamental differences in G.

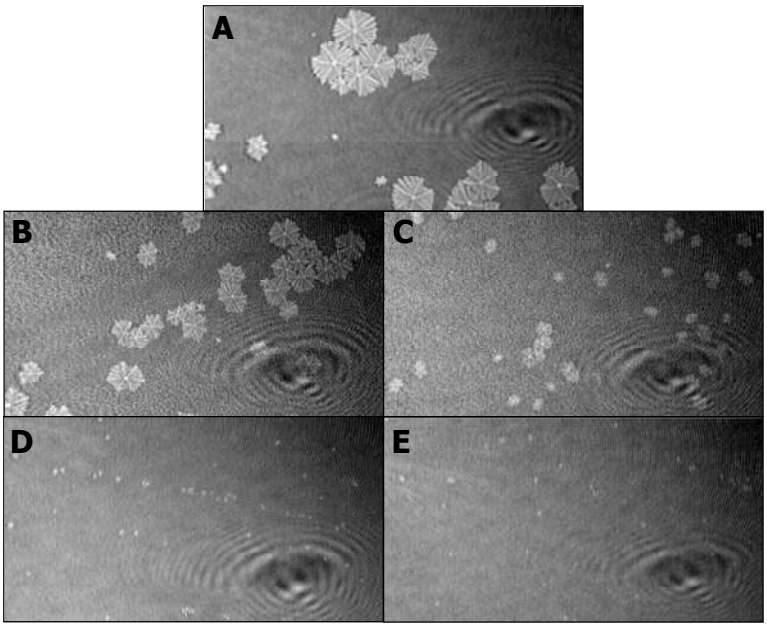


**Figure 6.7.** BAM images for $X_{PtBA}$ ~ 0.14 PCL/PtBA blends obtained at T = 22.5 °C for different compression rates: (A) 8, (B) 16, (C) 30, (D) 130, and (E) 200 $cm^2 \cdot min^{-1}$. All images were taken at surface area of <A> ~ 9-10 $Å^2 \cdot monomer^{-1}$. Solid-like domains appear bright in all of the 4.8 × 2.6 $mm^2$ BAM images.

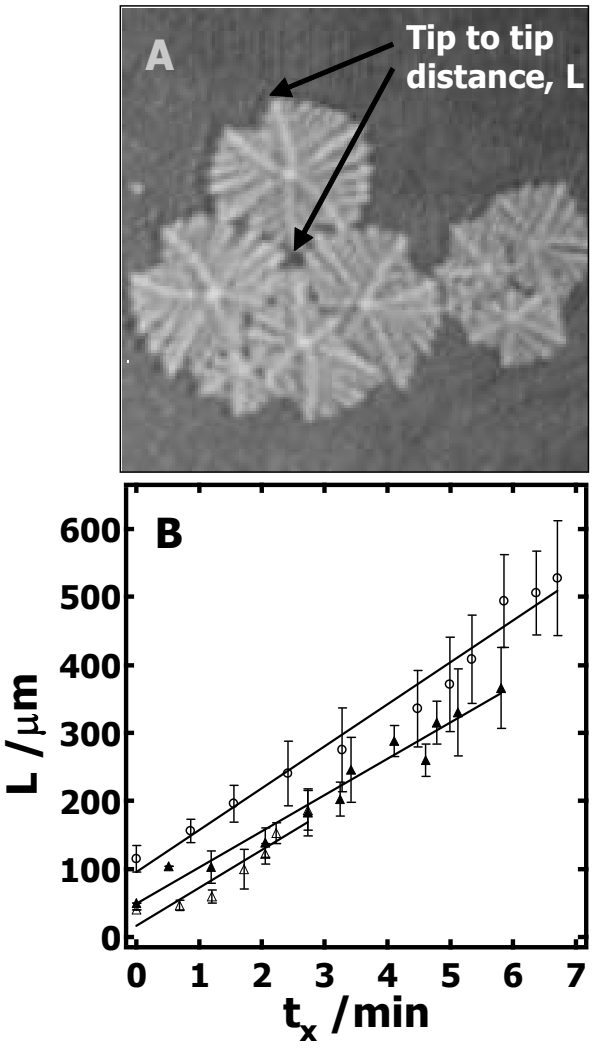


**Figure 6.8.** (A) A 1.6 × 1.6 $mm^2$ BAM image is used to highlight the measured linear dimension for a dendritic crystal. (B) Average tip to tip length, L, versus crystallization time, $t_x$ for PCL dendrites grown at T = 22.5 °C for different compression rates: 8 (○), 16 (▲), and 30 (Δ) $cm^2 \cdot min^{-1}$. Solid lines represent the linear fit used to estimate the average growth rate. Error bars on the individual data points represent ± one standard deviation following the procedure outlined in the text.

**Table 6.1.** Average growth rates for PCL dendrites grown at different compression rates.

| Compression rate | G |
|---|---|
| $cm^2 \cdot min^{-1}$ | $\mu m \cdot min^{-1}$ |
| 8 | 62 ± 4 |
| 16 | 53 ± 3 |
| 30 | 56 ± 9 |

Error bars represent ± one standard deviation.

### 6.3.3. Surface Pressure Dependence (Undercooling)

In Chapter 5, we examined the composition dependent growth of PCL dendrites in PCL/PtBA blend Langmuir films. In this chapter, the effects of multiple hysteresis loops and compression rate have also been considered. In this section, morphological studies for PCL dendrites grown in supersaturated monolayers during isobaric (constant Π) area relaxation experiments were used to explore the Π dependence of dendritic morphologies. For isothermal crystallization (T = 22.5 $^oC$) of PCL in Langmuir films, Π can be correlated to the degree of undercooling. Higher Π values are equivalent to higher degrees of undercooling. The isobaric area relaxation experiments were performed for $X_{PtBA}$ ~ 0.14 PCL/PtBA blends at target Π values of ~ 11, 10.5, 10.3, 10, 9.5, and 8.5 $mN \cdot m^{-1}$. The detailed experimental method has been described in Chapter 3. The target Π value for each isobaric area relaxation experiment is indicated on Π-<A> isotherms in Figure 6.9.

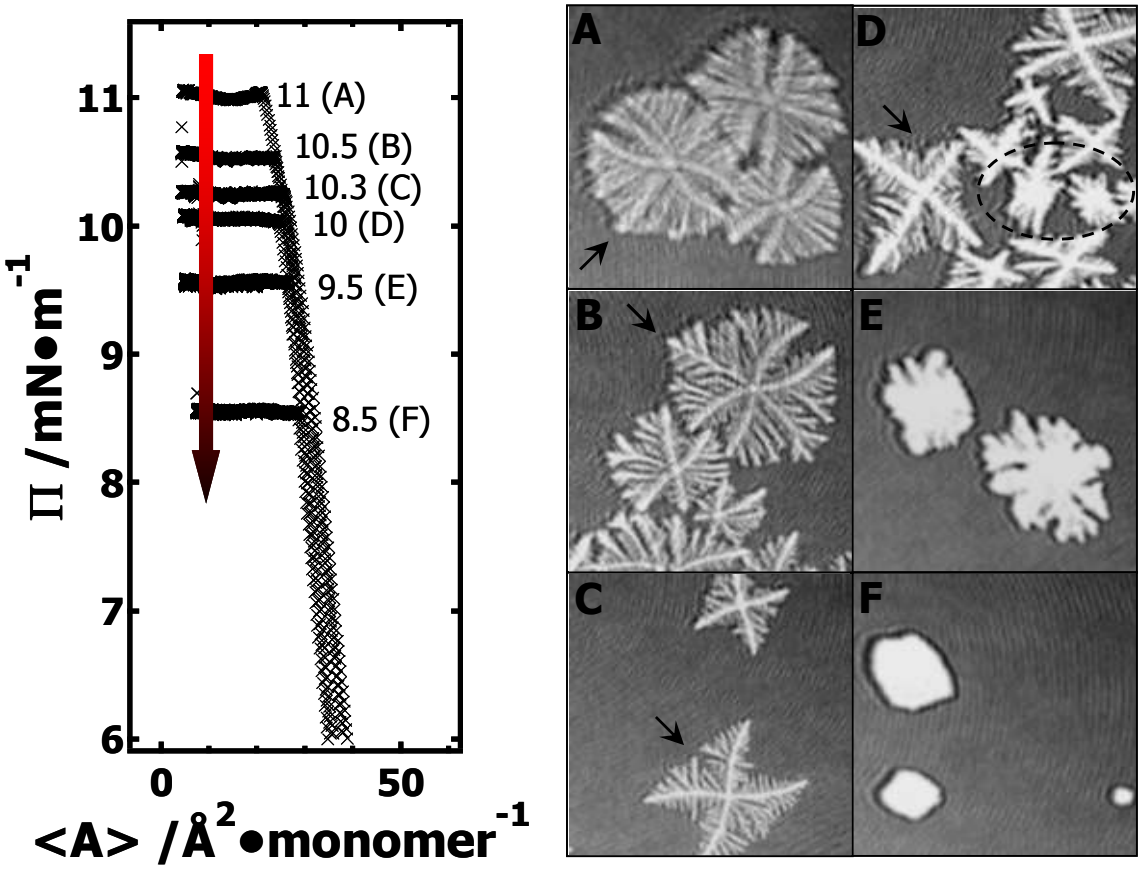


**Figure 6.9.** BAM images for $X_{PtBA}$ ~ 0.14 PCL/PtBA blends at 22.5 °C obtained during isobaric area relaxation experiments. Experiments were performed at ($\Pi$ /mN·m$^{-1}$): (A) 11, (B) 10.5; (C) 10.3, (D) 10, (E) 9.5, and (F) 8.5. BAM images were taken at <A> ~ 8-10 Å$^2$·monomer$^{-1}$ and also represent different crystallization time (time/hour): (A) 0.3, (B) 0.7; (C) 1.5, (D) 2.7, (E) 6.8, and (F) 7.6. The time scale indicated here represents the time for nucleation and growth instead of total relaxation time. Solid-like domains appear bright in all of the 1.6 × 1.6 mm$^2$ BAM images. The morphological transition of the "winning" branches in {100} sectors are indicated by arrows in BAM images A through D. The circle in image E indicates the presence of irregular branched crystals.

Figure 6.9A shows a BAM image taken during an isobaric area relaxation experiment at $\Pi \sim 11$ mN·m$^{-1}$, equivalent to a relatively high degree of undercooling. The BAM image clearly shows the dendritic branches in the {100} sectors grow faster than in the {110} sectors. The reason for the faster growth rate is that a greater pool of crystallizable polymer chains are present in the growth front of the {100} sectors. The length of all sidebranches in each {100} sector show an almost symmetric parabolic size distribution, leading to a maximum interfacial area between growing dendrites and the surrounding monolayer reservoir, which is statistically preferred to maximize the number of crystallizable PCL chains in the diffusion field. The detailed morphological features of PCL dendrites grown at $\Pi \sim 11$ mN·m$^{-1}$ have also been captured by optical microscopy (OM) performed on crystallized films that were transferred to solid substrates by the Langmuir-Schaefer (LS) method (Figure 6.10). Both Figure 6.9A and Figure 6.10A indicates that the growth of four main dendritic trunks, corresponding to the boundary lines between {100} and {110} sectors, are forced toward preferred directions. As a result, the diffusion of PCL chains from monolayers to the growth fronts of secondary sidebranches in {110} sectors is even more spatially hindered. Figure 6.10B shows dendritic tips of secondary sidebranches in a {100} sector. Growth directions of small sidebranches that develop along the tertiary branches are all pointed toward the growth front of the dendrites as indicated by the arrow in Figure 6.10B. In addition, the dendritic crystals that form at $\Pi \sim 11$ mN·m$^{-1}$ are highly branched, indicating a higher level of interfacial instability. Increasing the degree of undercooling associated with a higher crystallization pressure leads to a smaller self-diffusion coefficient, D, and greater growth rate, G. Thus, the diffusion length, given by $l_D = 2D/G$, decreases with increasing

degrees of undercooling.[122] As a consequence, the stability length also decreases, $\lambda_s \sim l_D^{1/2}$, leading to the highly branched dendrites seen in Figure 6.10.

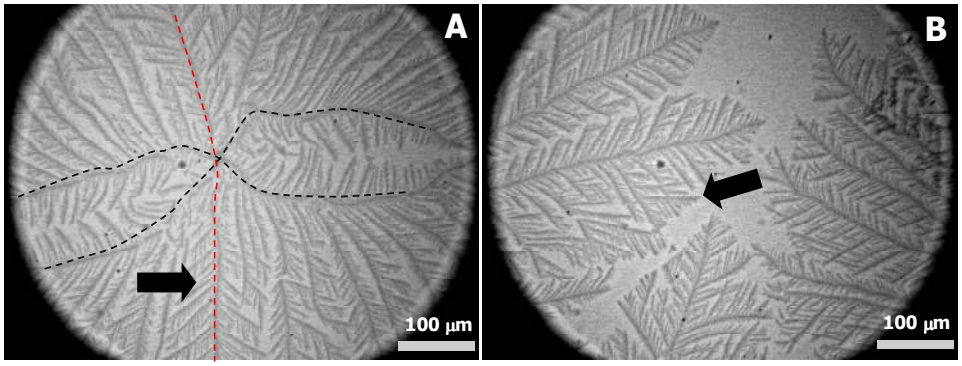


**Figure 6.10.** OM images of a single layer LS-film for a $X_{PtBA} \sim 0.14$ PCL/PtBA blend. The LS films were transferred onto PS coated silicon substrates at $\langle A \rangle \sim 5$ Å$^2$·monomer$^{-1}$ during an isobaric area relaxation experiment at $\Pi \sim 11$ mN·m$^{-1}$: (A) Symmetric dendritic branching, a "winning" branch is indicated by the arrow; and (B) Detailed features of dendritic tips. A dendritic tip is indicated by the arrow.

At lower $\Pi \sim 10.5$ mN·m$^{-1}$, corresponding to a lower degree of undercooling or a smaller supersaturation, the dendritic morphologies demonstrate two advanced branches in two {100} sectors as seen in Figure 6.9B and Figure 6.11. These two winning branches can escape the overlapping diffusion fields with their nearby dendritic arms. As a result, the "tertiary" sidebranches developed along these two branches can eventually impede the growth of the sidebranches grown on the main dendritic trunks as indicted in Figure 6.9B and Figure 6.11A. This morphological feature is very similar to the dendritic

morphologies observed for $X_{PtBA}$ ~ 0.26 PCL/PtBA blends shown in Chapter 5, suggesting that decreasing Π may be comparable to increasing the composition of amorphous phase with respect to morphological evolution. Further decreasing the crystallization surface pressure down to Π ~ 10.3 $mN \cdot m^{-1}$ leads to the appearance of four-arm dendritic crystals as seen in Figure 6.9C and Figure 6.12. The winning branches once observed at Π ~ 10.5 $mN \cdot m^{-1}$ in {100} sectors are no longer present and were essentially cut-off by the secondary sidebranches developed along main dendritic trunks as indicated by the arrow in Figure 6.12. In this case, the secondary sidebranches in the {110} sectors possess a higher probability of incorporating crystallizable material from the surrounding monolayer, thereby growing faster than at higher degrees of undercooling.

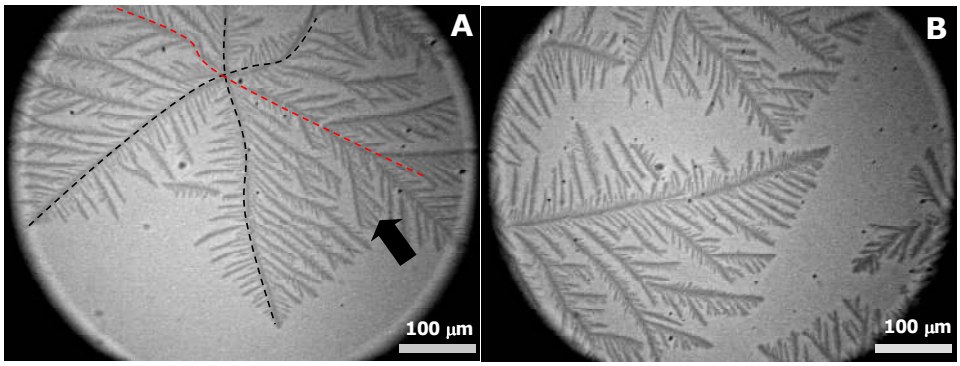


**Figure 6.11.** OM images of a single layer LS-film for a $X_{PtBA}$ ~ 0.14 PCL/PtBA blend. The LS films were transferred onto PS coated silicon substrates at <A> ~ 5 $Å^2 \cdot monomer^{-1}$ during an isobaric area relaxation experiment at Π ~ 10.5 $mN \cdot m^{-1}$: (A) Symmetric dendritic branching, a "winning" branch is indicated by the arrow; and (B) Detailed features of a dendritic tip.

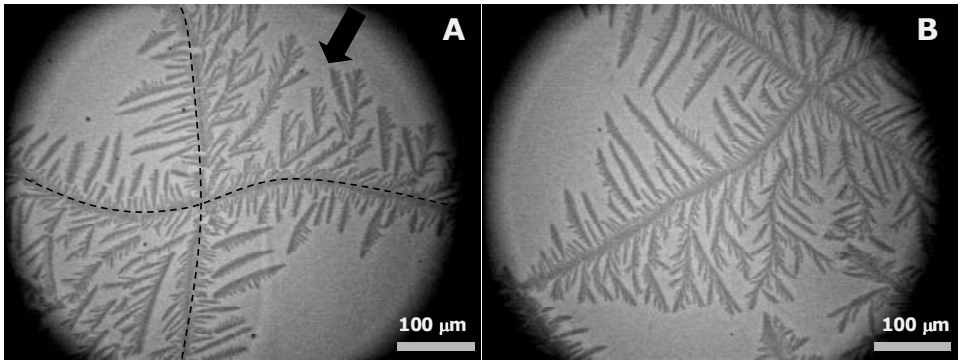


**Figure 6.12.** OM images of a single layer LS-film for a $X_{PtBA}$ ~ 0.14 PCL/PtBA blend. The LS films were transferred onto PS coated silicon substrates at <A> ~ 5 $Å^2$·monomer$^{-1}$ during an isobaric area relaxation experiment at Π ~ 10.3 mN·$m^{-1}$: (A) Symmetric dendritic branching, dendritic branches in one {100} sector are indicated by the arrow; and (B) Detailed features of a dendritic tip.

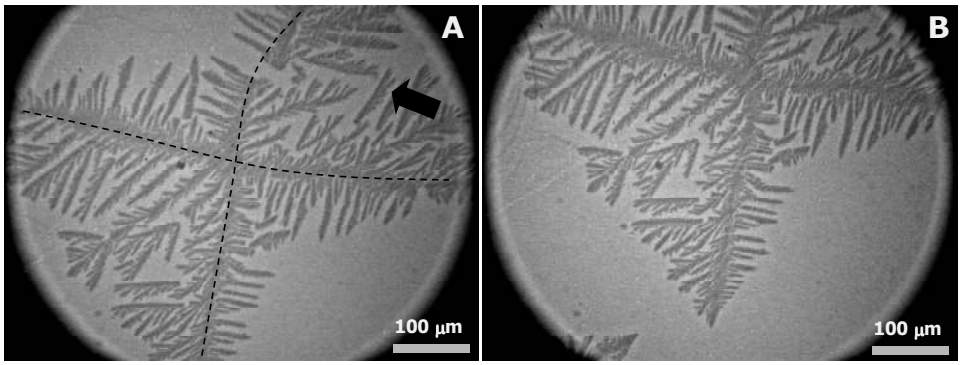


**Figure 6.13.** OM images of a single layer LS-film for a $X_{PtBA}$ ~ 0.14 PCL/PtBA blend. The LS films were transferred onto PS coated silicon substrates at <A> ~ 5 $Å^2$·monomer$^{-1}$ during an isobaric area relaxation experiment at Π ~ 10 mN·$m^{-1}$: (A) Symmetric dendritic branching, dendritic branches in one {100} sector are indicated by the arrow; and (B) Detailed features of a dendritic tip.

At even lower crystallization Π of ~ 10 $mN \cdot m^{-1}$, four-arm dendrites are found to coexist with even more fully developed crystals like the ones circled in Figure 6.9D. Sidebranches developed along the four primary dendritic trunks demonstrate similar features to those observed at Π ~ 10.3 $mN \cdot m^{-1}$ in Figure 6.12, while the fully developed crystals show more randomly-branched fat fingers without any preferential orientation in space. Similar morphologies were also observed during isobaric crystallization at Π ~ 9.5 $mN \cdot m^{-1}$ (Figure 6.9E and Figure 6.14). The development of sidebranches in this case should be more hindered because the stability length increases with decreasing degrees of undercooling. PCL crystals grown at Π ~ 8.5 $mN \cdot m^{-1}$ show distorted rectangular morphologies as seen in Figure 6.9F and Figure 6.15. The morphological transitions for PCL dendrites from highly branched symmetric dendrites to distorted rectangular shapes are comparable to it-PS system reported by Taguchi *et al.*[122] However, the morphological evolution in the PCL system associated with different growth rates in the {100} and {110} sectors is obviously more complicated than in the highly symmetric it-PS system.[122] For the nonequilibrium pattern formation of dendritic crystals, important controlling factors include the degree of undercooling and its interplay with diffusion properties, interfacial tension, and interfacial tension anisotropy. The interfacial tension tends to stabilize the solid/liquid interface during crystallization. The interfacial tension anisotropy represents an orientational dependence of the interfacial tension and increases with decreasing degree of undercooling. For polymeric systems, the interfacial tension anisotropy has not been experimentally measured, although it has been used as a parameter by theoretical chemists to induce morphological transitions in the diffusion-limited growth regime for systems with different degrees of undercooling. Further theoretical and experimental studies are still required to understand the origin of this

unique morphological transition for PCL dendrites at the A/W interface. Proposed experiments to further elucidate these questions are included in Chapter 9.

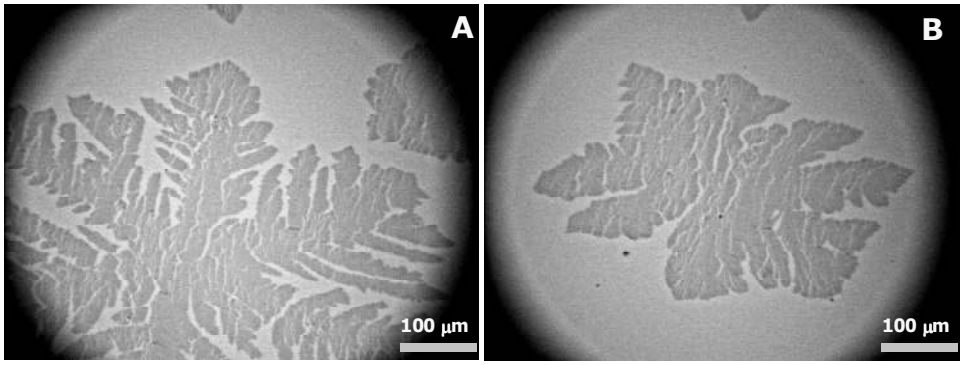


**Figure 6.14.** OM images of a single layer LS-film for a $X_{PtBA}$ ~ 0.14 PCL/PtBA blend. The LS films were transferred onto PS coated silicon substrates at <A> ~ 5 $Å^2$·monomer$^{-1}$ during an isobaric area relaxation experiment at Π ~ 9.5·$m^{-1}$. Both (A) and (B) show fat dendritic fingers.

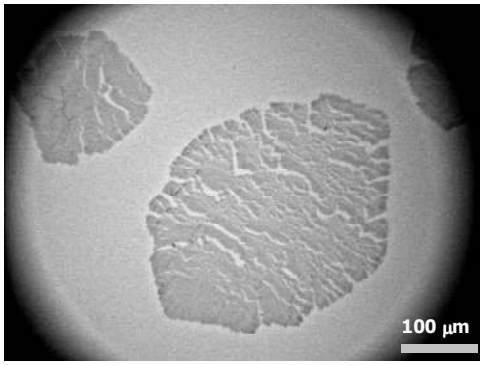


**Figure 6.15.** OM image of a single layer LS-film for a $X_{PtBA}$ ~ 0.14 PCL/PtBA blend. The LS film was transferred onto a PS coated silicon substrates at <A> ~ 8 $Å^2$·monomer$^{-1}$ during an isobaric area relaxation experiment at Π ~ 8.5 mN·$m^{-1}$.

Furthermore, representative BAM images obtained at $\Pi \sim 10.5$ mN·m$^{-1}$ shown in Figure 6.16A through F were used to examine the growth process for PCL dendrites during isobaric area relaxation experiments. Plots of $<A>-<A>_0$ as a function of relaxation time are also shown in Figure 6.16. $<A>_0$ is the initial surface area, corresponding to the starting point for the relaxation experiment at $\Pi \sim 10.5$ mN·m$^{-1}$. The letters on the $<A>-<A>_0$ vs. time plot indicates when the BAM images A trough F were taken. It is interesting to note that at the early stage of crystallization, the dendritic trunks grown on the boundary lines between the {100} and {110} sectors are straight and reflect the symmetry of PCL crystal structure as shown in Figure 6.16A and B. Figure 6.16A and B also show that the leading branches in the {100} sectors start growing almost simultaneously with the four primary dendritic trunks, suggesting that these leading sidebranches are developed on unstable crystal faces instead of the surfaces of primary dendritic trunks. The growth rate of secondary sidebranches in the {110} sectors seems to be substantially smaller than in the {100} sectors. As a result, the growth fronts of the four dendritic trunks start to bend toward the dividing line between {110} sectors as seen in Figure 6.16C and more clearly in Figure 6.16D through F. Consequently, the growth direction of the secondary sidebranches developed along the primary dendritic trunks in {110} sectors change to maintain a branching angle that is perpendicular to the growth fronts.

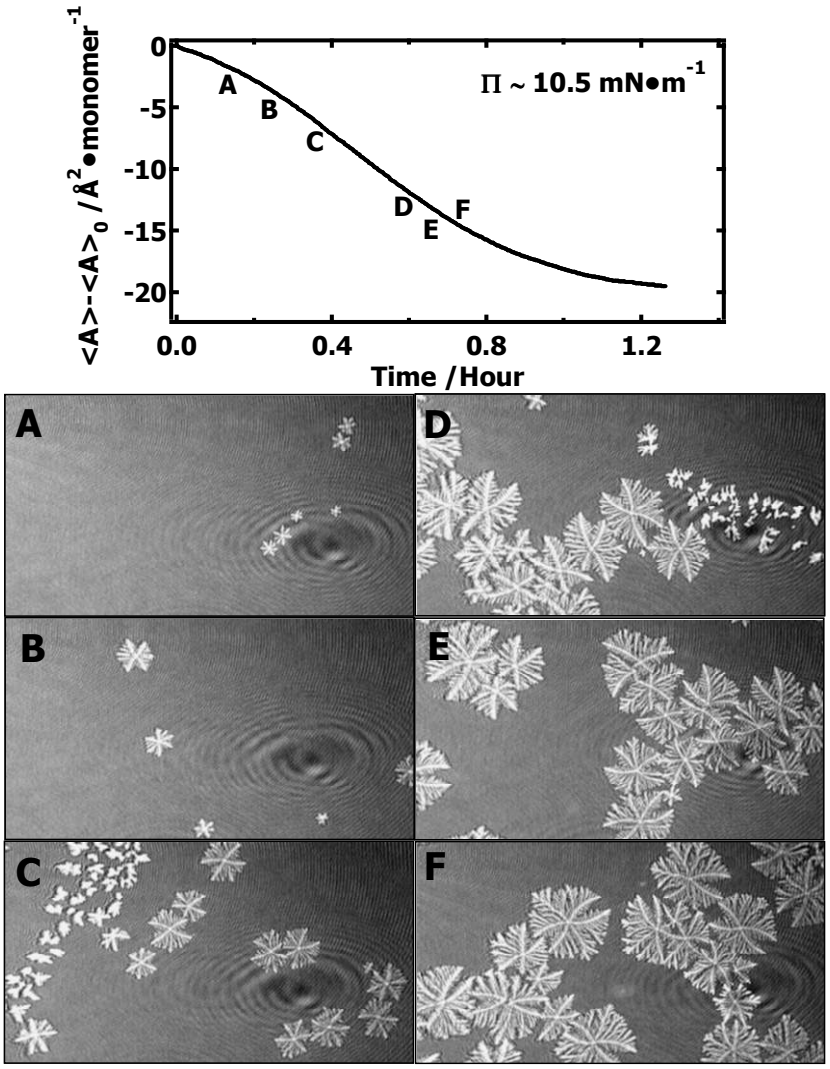


**Figure 6.16.** BAM images for a PCL/PtBA blend of $X_{PtBA}$ ~ 0.14 obtained during isobaric area relaxation experiments at Π ~ 10.5 mN·m$^{-1}$. BAM images were taken during isobaric experiments at (Time /hour): (A) 0.14, (B) 0.25, (C) 0.37, (D) 0.59, (E) 0.66 and (F) 0.70. Solid-like domains appear bright in all of the 4.8 × 2.6 mm$^2$ BAM images.

While BAM experiments do not allow one to follow the growth of a single dendrite, the measurement methods discussed above in Section 6.2 can still be used to estimate an average growth rate at different Π. The tip-to-tip distance of PCL dendrites, L, is plotted as a function of $t_x$ in Figure 6.17. The growth is roughly linear at early times. The slopes of linear fits of L vs. $t_x$, $G = dL/dt_x$, indicate the growth rate increases with increasing Π as seen in Table 6.2.

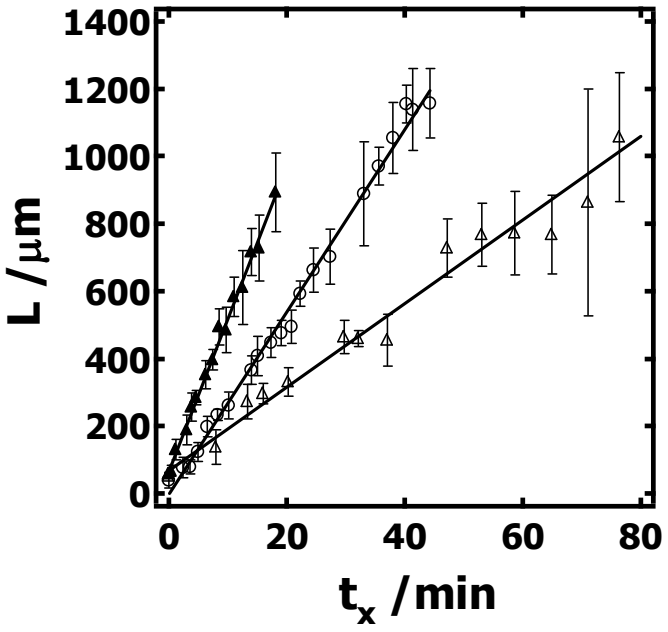


**Figure 6.17.** Average tip to tip length, L, versus crystallization time, $t_x$, for PCL dendrites grown during isobaric area relaxation experiments at different Π: 11 (▲), 10.5 (○), and 10.3 (Δ) $mN \cdot m^{-1}$. Solid lines represent the linear fit used to estimate the average growth rate. Error bars on the individual data points represent ± one standard deviation following the procedure outlined in the text.

**Table 6.2.** Average growth rates for PCL dendrites grown at different surface pressures.

| **Target Π** | **G** |
|---|---|
| $mN \cdot m^{-1}$ | $\mu m \cdot min^{-1}$ |
| 11 | 45 ± 1 |
| 10.5 | 27 ± 1 |
| 10.3 | 12 ± 1 |

Error bars represent ± one standard deviation.

## 6.4. Conclusions

In summary, morphological features of PCL crystals grown in PCL/PtBA Langmuir films at different experimental conditions were extensively examined. Multiple hysteresis experiments indicate that PCL crystals grown during the first compression step do not completely melt during expansion and the locally well-ordered 3D structures serves as nuclei for crystallization during the second compression step, leading to more and smaller crystals during the second compression step. It is also found that increasing compression rate suppresses PCL crystallization. At higher compression rates, polymer chains have less time to nucleate and grow crystals for compression to the same <A>, i.e. shorter $t_x$, leading to poorer chain organization in crystallites, smaller crystal sizes, and higher melting Π (analogous to lower melting point). Furthermore, morphological results obtained from isobaric area relaxation experiments at different Π values demonstrate a transition from highly branched symmetric dendrites to six-arm dendrites, four-arm dendrites, seaweedlike crystals, and distorted rectangular crystals, indicating that the degree of undercooling plays a key role for controlling crystal morphologies through the interplay of the diffusion coefficient, interfacial energy, and interfacial energy anisotropy. In addition, the noise level (compositional fluctuations) varies with crystallization Π and

the blend composition, which can be considered as another effective parameter for morphological selection in the diffusion-limited growth regime. The morphological transition of PCL dendrites has not been previously reported. Further experimental and theoretical studies on this interesting model system are important to fully understand the morphological development in the diffusion-limited regime.